RSC Advances

PAPER

View Article Online
View Journal | View Issue

Check for updates

Cite this: *RSC Adv.*, 2026, **16**, 15831

Molecular dynamics insights into combustion mechanisms of JP-10/aluminum nanoparticle composite fuels

Mengfan Si, Shuai Wang, Haiou Wang, Hanhui Jin, Kun Luo and Jianren Fan *

The incorporation of metal nanoparticles can enhance the energy release and ignition performance of high-energy-density fuels; however, the effects of particle aggregation and sedimentation mechanisms on combustion remain insufficiently understood. In this work, reactive molecular dynamics simulations are employed to investigate the ignition and combustion behaviors of JP-10/Al composite systems. A validated JP-10/Al model is constructed, and ignition delay, reaction kinetics, and structural descriptors are analyzed across a temperature range of 2000–3000 K and Al concentrations of 10–40 wt%. The results reveal that Al nanoparticle morphology evolves from chain-like extensions to fragmentation and eventual secondary aggregation. The presence of Al accelerates reactant consumption, shortens ignition delay, and promotes rapid Al–O and Al–C bond formation, which destabilizes JP-10 and facilitates cage ring-opening. The accelerated generation of reactive fragments reduces the apparent activation energy by 49.8%. Increasing Al concentration further emphasizes the trade-off: while low-to-moderate loadings enhance ignition, excessive additions induce severe aggregation and reduce efficiency. An optimal concentration window of 20–25 wt% is identified, balancing ignition promotion with minimal aggregation losses. These findings provide mechanistic insights into the multiscale combustion processes of JP-10/Al systems and offer guidance for the design of high-performance composite fuels in aerospace propulsion.

Received 3rd January 2026
Accepted 5th March 2026

DOI: 10.1039/d6ra00051g

rsc.li/rsc-advances

Open Access Article. Published on 20 March 2026. Downloaded on 5/18/2026 10:20:52 PM.
This article is licensed under a Creative Commons Attribution-NonCommercial 3.0 Unported Licence.

1. Introduction

High-energy suspension fuels are composite fuels formed by dispersing metal particles into liquid fuels. As shown in Fig. 1, they combine the flowability of liquid fuels with the high energy density of metals, offering a promising strategy to enhance the energy density and combustion performance of conventional propellants.[1] Such fuels have been applied in aerospace propulsion, high-speed flight, and military systems. However, their combustion process is inherently complex. It typically involves sequential stages, including evaporation and decomposition of the liquid phase, heating and oxidation of metal particles, and possible particle agglomeration and phase transitions. These strongly coupled multiphase processes are sensitive to key parameters such as metal concentration and temperature.[2] Variations in these conditions directly influence ignition delay, heat release rate, and combustion completeness. Moreover, the high thermal conductivity and reactivity of metal particles alter the reaction pathways and product evolution, introducing additional uncertainty. Therefore, a clear understanding of the fundamental mechanisms governing combustion behavior under different conditions is essential for fuel design and propulsion optimization.

Numerous experimental studies have been carried out to explore the combustion characteristics and performance of liquid fuels enhanced with metal-based energetic additives. Luo *et al.*[3] investigated the combustion behavior of JP-10-based slurries containing nanosized aluminum particles, analyzing post-combustion residues *via* XRD, SEM, and TGA, and identified evident particle agglomeration and incomplete oxidation. Jin *et al.*[4] evaluated a JP-10 slurry with 16 wt% Al nanoparticles in a scramjet engine and reported significant enhancements in combustion efficiency and density-specific impulse, with improvements up to 34.37%, demonstrating its applicability in

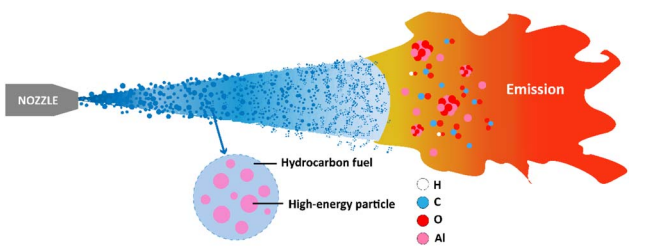

Fig. 1 Schematic of the atomization and combustion of high-energy fuels.

State Key Laboratory of Clean Energy Utilization, Zhejiang University, Hangzhou 310027, China. E-mail: fanjr@zju.edu.cn; Fax: +086-87953687; Tel: +086-87953687

© 2026 The Author(s). Published by the Royal Society of Chemistry

Open Access Article. Published on 20 March 2026. Downloaded on 5/18/2026 10:20:52 PM. This article is licensed under a Creative Commons Attribution-NonCommercial 3.0 Unported Licence.

high-speed propulsion systems. In the context of diesel blends, Gad *et al.*[5] observed that the inclusion of 40 ppm alumina nanoparticles led to a 5.5% rise in thermal efficiency and notable reductions in HC, CO, and NOx emissions by as much as 33%, along with shortened ignition delay. Similarly, Mostafa *et al.*[6] employed response surface methodology (RSM) to assess Al_2O_3-modified diesel performance and found that a 50 ppm concentration enhanced brake thermal efficiency by 4.91% and reduced key emissions significantly under high load conditions. Complementing these findings, Chen *et al.*[7] developed JP-10-based gel fuels incorporating up to 30 wt% Al or B particles using a low-molecular-weight gellant, achieving favorable thixotropic behavior, structural stability, and energy performance, with increases in density and net heat of combustion reaching 30% and 43%, respectively. Experimental studies have offered valuable insights into the combustion behavior of high-energy suspension fuels. However, limitations in experimental setups and cost restrict the exploration of wide-ranging operating conditions. Moreover, such methods lack the resolution to uncover molecular-scale mechanisms, underscoring the necessity of simulation-based approaches. Yang *et al.*[8] investigated the use of calcium fluoride (CaF_2) to modify nanometric aluminum (nAl) for enhancing JP-10 fuel performance. Their study revealed that CaF_2 coating effectively inhibited surface oxidation, accelerated droplet vaporization, and promoted micro-explosions. Most significantly, the CaF_2-modified nAl substantially reduced the ignition delay time by 50% and lowered the ignition temperature by approximately 43% in Al/JP-10 nanofluid fuel droplets. These findings offer strong theoretical support for the application of inorganic fluoride-modified Al nanoparticles in liquid hydrocarbon fuels. Zhang *et al.*[9] investigated the enhancement of Al–Li alloy powder (Al–Li5) stability and combustion performance *via* polyurethane (PU) coating. To address the high reactivity and poor compatibility of Li, they synthesized PU *in situ* using isophorone diisocyanate and ethylene glycol to encapsulate the alloy particles. The resulting Al–Li5@PU composite demonstrated significantly improved stability, thermal response, and notably, a shortened ignition delay along with higher combustion efficiency. This approach provides a practical foundation for advancing Al–Li alloy applications in high-energy propulsion systems. Yang *et al.*[10] investigated the combustion enhancement of boron (B) powder through surface coating with aluminum (Al) to disrupt its inhibitory oxide layer. Their study revealed that an optimal Al content significantly lowered the oxidation temperature and increased heat release of B powder, while excessive Al deteriorated combustion performance but suppressed particle aggregation. The interfacial reactions between Al and B accelerated combustion and improved efficiency, providing a foundation for the application of B@Al composites in energetic materials.

Reactive molecular dynamics, as an advanced simulation approach, offers a robust framework for investigating chemically reactive systems at the atomic scale. By explicitly capturing bond breaking and formation events, it enables detailed tracking of complex reaction pathways during combustion. This method is particularly suited for modeling multiphase systems under extreme conditions, such as high temperatures, elevated pressures, and rapid energy release. In recent years, reactive molecular dynamics simulations have been increasingly applied to probe the combustion characteristics, oxidation mechanisms, and structural evolution of high-energy materials[11] and nanoparticle-suspended fuels.[12]

One important research direction focuses on metal-based particles and their derivatives, aiming to elucidate their intrinsic combustion and oxidation behaviors. For example, Feng *et al.*[13] investigated the decomposition and oxidation of AlH_3, revealing a three-stage reaction process and the retarding effect of oxide layers on hydrogen release. Wang *et al.*[14] studied Ni nanoparticle oxidation and uncovered a surface nucleation–growth–inward diffusion sequence sensitive to environmental conditions. Song *et al.*[15] analyzed Al–Mg alloy nanoparticles and reported a distinct phase separation followed by the formation of hollow-shell structures during oxidation. Jiang *et al.*[16] explored the initial wet oxidation of Fe–Cr alloys and demonstrated how Cr enrichment and water dissociation drive the formation of protective oxide films. Xiong *et al.*[17] investigated the optimization of fluorinated graphene (FG) content in Al/FG composites to enhance combustion performance. Through combined experiments and ReaxFF molecular dynamics simulations, they revealed that an FG content of approximately 30 wt% yields optimal reaction characteristics, whereas excessive FG reduces system energy density.

A parallel line of studies has turned to the combustion behavior of particle-suspended fuels, with a particular focus on nanofluid systems. These systems integrate reactive nanoparticles into conventional or alternative fuels, enabling enhanced energy release and combustion control. Zhang *et al.*[18] investigated ethanol oxidation on Al nanoparticles and found that oxidation onset temperature is significantly reduced, with oxide thickness modulating the dominant reaction pathways. Cheng *et al.*[19] simulated ANP/n-butanol fuels and identified a three-stage combustion process, showing that ANPs reduce ignition delay, suppress sintering, and improve combustion completeness. In a follow-up study, Cheng *et al.*[20] demonstrated that AlH_3 not only promotes ethanol decomposition but also reduces activation energy by 12.7%, leading to Al_2O_3 formation as the dominant residue. Zhao *et al.*[21] revealed a four-stage combustion mechanism in methanol-Al nanofluids, emphasizing enhanced radical formation and micro-explosion behavior. Lu *et al.*[22] explored the use of oleic acid (OA) to modify aluminum nanoparticles (ANPs) in order to enhance the combustion performance of Al/JP-10 fuel. They found that surface modification with OA improved the dispersion and oxidation resistance of ANPs, effectively inhibiting agglomeration and protecting the aluminum core. At elevated temperatures, the Al@OA particles accelerated the exothermic oxidation process, significantly shortening the ignition delay and intensifying the combustion of JP-10 droplets. The optimal performance was achieved with an Al : OA ratio of 10 : 3, which resulted in the shortest ignition delay. Kong *et al.*[23] examined how the oxidation degree of aluminum nanoparticles (ANPs) affects the performance of Al/JP-10 nanofluid fuels. They found that increased oxidation promotes ANP agglomeration, reduces fuel stability, and significantly prolongs ignition delay. The

© 2026 The Author(s). Published by the Royal Society of Chemistry

Open Access Article. Published on 20 March 2026. Downloaded on 5/18/2026 10:20:52 PM. This article is licensed under a Creative Commons Attribution-NonCommercial 3.0 Unported Licence.

oxide layer also hinders the core aluminum reaction, impairing combustion. Notably, the impact of ANP oxidation on JP-10 decomposition shifted from inhibitory at 2000 K to catalytic at 3000 K. Zhao *et al.*[24] further examined Al/ethanol nanofluids and identified multiple enhancement mechanisms-ranging from chain reactions to melt dispersion-depending on particle size and oxidation state. Complementarily, Chen *et al.*[25] studied Al nanoparticle agglomeration under combustion-relevant conditions and showed that reduced oxide integrity and smaller particle sizes facilitate clustering, ultimately diminishing combustion efficiency.

ReaxFF-based molecular dynamics has been extensively applied to investigate combustion- and oxidation-related processes involving metallic species, particularly focusing on metal particle oxidation dynamics and metal-assisted combustion phenomena in hydrocarbon or oxygen-rich environments. These studies have provided important insights into bond evolution characteristics, reaction pathways, and the role of metallic additives at elevated temperatures, forming a methodological and mechanistic basis for molecular-level analysis of metal-fuel interactions under reactive conditions. Despite significant progress, several limitations remain in the current body of ReaxFF-based combustion studies. Most existing work centers on metal particle oxidation or alcohol-based nanofluid fuels, with limited attention paid to high-energy hydrocarbon systems such as JP-10. The interactions between metallic additives and complex fuel molecules under combustion conditions remain poorly characterized, particularly regarding their effects on ignition delay, combustion efficiency, and molecular-scale reaction pathways. Furthermore, few studies have systematically explored the influence of particle concentration or identified optimal mixing ratios. These gaps highlight the need for more comprehensive simulations that capture the coupled effects of molecular composition, additive concentration, and combustion dynamics in realistic multiphase fuels.

To address these challenges, this study constructs a high-energy suspension fuel model composed of JP-10 and nano-aluminum particles, and investigates its combustion behavior under varied temperatures and aluminum concentrations using reactive molecular dynamics (ReaxFF) simulations. The insights gained aim to support enhanced ignition control by reducing ignition delay, and to improve energy release efficiency through optimal nanoparticle incorporation and dispersion. The novelty of this work lies in two aspects: (i) the establishment of a molecular-level model of JP-10/nano-Al fuels with tunable metal loadings representative of real propellant formulations; and (ii) the mechanistic elucidation of combustion enhancement pathways, including radical generation, structural evolution, and particle interactions across a range of thermal conditions. The remainder of this paper is structured as follows. After Introduction section, Section 2 introduces the modeling methodology and force field validation. Section 3 outlines the simulation protocols, including system composition and thermodynamic settings. Section 4 presents the combustion results, covering ignition delay, heat release, and reaction pathways. Section 5 concludes with key findings and design recommendations for metalized fuel systems.

2. Methodology

2.1 Reactive molecular dynamics (MD) model

ReaxFF (Reactive Force Field) is a bond-order-based empirical force field developed to enable the modeling of chemical reactions within classical molecular dynamics (MD) simulations.[26] Its predictive accuracy bridges the gap between conventional MD and quantum mechanical (QM) methods, offering a compelling compromise between computational efficiency and the ability to describe reactive events with atomistic fidelity. In contrast to traditional MD force fields that rely on fixed, predefined bonds, ReaxFF employs a continuously varying bond order formalism that allows for the dynamic formation and dissociation of chemical bonds during simulations. This feature makes it particularly well-suited for capturing the reaction kinetics of gas, liquid, solid, and multiphase systems under chemically reactive conditions.

With its robust capability to capture chemical transformations and its high parameter transferability, the ReaxFF method has been extensively utilized in atomistic simulations of chemically reactive systems. In the context of hydrocarbon oxidation and combustion chemistry, ReaxFF has been successfully applied to investigate reaction mechanisms such as bond activation, chain branching, and oxidation pathways.[27] For surface and interfacial reactive phenomena, ReaxFF enables detailed simulations of adsorption, bond dissociation, and gas–solid or solid–liquid interactions under realistic thermodynamic conditions.[28–31] In addition, ReaxFF has been widely employed to study high-temperature reactive transformations and the formation and condensation of carbonaceous structures under extreme conditions.[32]

The ReaxFF force field is based on a reactive bond-order formalism combined with an electronegativity equalization method (EEM), which enables a continuous description of bond breaking and formation as well as dynamic charge redistribution during chemical reactions. The parameters of the ReaxFF potential are calibrated against extensive datasets derived from density functional theory (DFT) calculations, including molecular geometries, energies, and charge distributions, to ensure quantitative consistency with quantum-mechanical descriptions. This theoretical framework allows ReaxFF to model chemical reactivity without explicit electronic structure calculations, thereby extending accessible simulation timescales to the microsecond regime and spatial resolutions to the nanometer scale. Furthermore, the force field exhibits strong parameter transferability, enabling a single elemental parameter set (*e.g.*, oxygen) to consistently describe behavior across diverse chemical environments such as O_2 gas, liquid water, and solid oxides. This transferability enhances the robustness and generality of ReaxFF for cross-phase and multiscale simulations.

The total energy in ReaxFF is expressed as a sum of multiple energy contributions:

$$E_{\text{system}} = E_{\text{bond}} + E_{\text{over}} + E_{\text{angle}} + E_{\text{tors}} + E_{\text{vdWaals}} + E_{\text{Coulomb}} + E_{\text{Specific}} \quad (1)$$

Open Access Article. Published on 20 March 2026. Downloaded on 5/18/2026 10:20:52 PM. This article is licensed under a Creative Commons Attribution-NonCommercial 3.0 Unported Licence.

where E_{bond} accounts for the bond energy between atom pairs, derived from a continuous bond order formalism; E_{over}- introduces a penalty for over-coordination by suppressing unphysically high bond orders; E_{angle} and E_{tors} represent angular and torsional interactions among three or four atoms, respectively; $E_{vdWaals}$ and $E_{Coulomb}$ describe long-range nonbonded interactions, including van der Waals forces and electrostatics; and $E_{Specific}$ incorporates system-dependent terms such as hydrogen bonding, π–π stacking, or other specialized interactions.

The core of ReaxFF lies in the calculation of a continuous bond order BO_{ij}, which depends on the interatomic distance and atomic types. A typical functional form is given by:

$$\begin{aligned} BO_{ij}\ \& &= BO_{ij}^{\sigma} + BO_{ij}^{\pi} + BO_{ij}^{\pi\pi} \\ \& &= \exp\left[p_{bo1}\left(\frac{r_{ij}}{r_o^{\sigma}}\right)^{p_{bo2}}\right] + \exp\left[p_{bo3}\left(\frac{r_{ij}}{r_o^{\pi}}\right)^{p_{bo4}}\right] + \exp\left[p_{bo5}\left(\frac{r_{ij}}{r_o^{\pi\pi}}\right)^{p_{bo6}}\right] \end{aligned} \quad (2)$$

where r_{ij} is the interatomic distance, and r_o^{σ}, r_o^{π}, $r_o^{\pi\pi}$ represent the reference bond lengths for σ, π, and ππ interactions, respectively. The parameters $p_{boi}(i = 1–6)$ are fitted to high-level quantum mechanical data.

2.2 Model validation for JP-10-based system

In this work, a ReaxFF parameter set encompassing Al/C/H/O atomic interactions, originally developed by Hong *et al.*,[33] was adopted. To validate the ReaxFF force field for JP-10, the reaction energy barriers for key ring-opening pathways were validated against DFT calculations and showed satisfactory agreement; detailed comparisons are provided in Fig. S1 of the SI. As shown in Fig. 2, the atom numbering scheme of the JP-10 molecule was defined to facilitate direct comparison. The thermal stability and kinetic behavior of multi-molecular JP-10 systems under heating conditions are also presented in Fig. S2 of the SI.

2.3 Data analysis

Morphological analysis was conducted using OVITO to visualize the trajectory files obtained from the simulations, enabling intuitive observation of molecular structural evolution and the temporal progression of the reaction process.

Bond analysis was carried out by extracting bond connectivity data at representative timesteps to construct structural snapshots. These were then combined with atomic coordinates to calculate time-dependent variations in characteristic bond lengths and bond angles. Species analysis was performed based on the output species identification files to statistically monitor the formation and consumption of major intermediates and final products, such as H_2O, CO, CO_2, and Al_2O_3. This allowed for the identification of dominant reaction pathways and key combustion stages. Finally, cluster analysis was undertaken to trace the high-temperature behavior of aluminum particles, capturing their dynamic evolution-including fragmentation, recombination, and the formation of hollow structures-thus providing mechanistic insight into the structural response of metallic particles in multiphase reactive environments.

In addition, kinetic analysis was performed to quantitatively characterize the temperature-dependent decomposition behavior of JP-10. At each temperature, the remaining number of JP-10 molecules was statistically counted. Assuming a first-order reaction model, the reaction rate constant k was obtained by linear fitting of the temporal evolution of JP-10 molecular population according to:

$$\ln N_t - \ln N_0 = -kt \quad (3)$$

where $N_t$and N_0 denote the numbers of JP-10 molecules at time t and at the initial state, respectively.

Subsequently, the apparent activation energy E_a was determined using the Arrhenius relationship by linearly fitting ln k as a function of $1/T$:

$$\ln k = \ln A - \frac{E_a}{RT} \quad (4)$$

where A is the pre-exponential factor, R is the universal gas constant, and T is the absolute temperature. The slope of the fitted line yields $-E_a/R$, from which E_a can be directly calculated. This approach is widely adopted in reactive molecular dynamics studies and provides a physically meaningful description of molecular-scale reaction kinetics.

All the aforementioned analyses were performed using a self-developed data processing framework, which is capable of automatically recognizing, parsing, and visualizing various ReaxFF output files. This significantly enhanced the efficiency of structural analysis and deepened mechanistic understanding in complex reactive systems.

3. Computational settings

3.1 System construction

As shown in Fig. 3, to explore the combustion behavior of aluminum-suspended fuels, a series of multi-component reactive systems comprising JP-10, O_2, and nano-sized aluminum particles were constructed. A reference system containing only JP-10 and O_2 was also established to isolate and quantify the influence of aluminum on combustion characteristics. Aluminum nanoparticles were generated from a face-centered cubic (FCC) lattice and truncated into spherical clusters with a diameter of 4 nm, each comprising approximately 1985 atoms. This particle size was selected based on prior findings[34]

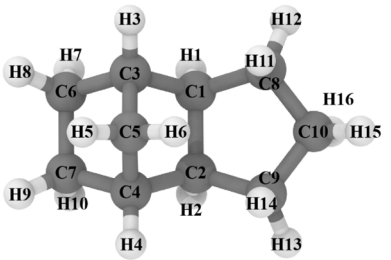

Fig. 2 Atom numbering scheme of the JP-10 molecule.

© 2026 The Author(s). Published by the Royal Society of Chemistry

Open Access Article. Published on 20 March 2026. Downloaded on 5/18/2026 10:20:52 PM.
This article is licensed under a Creative Commons Attribution-NonCommercial 3.0 Unported Licence.

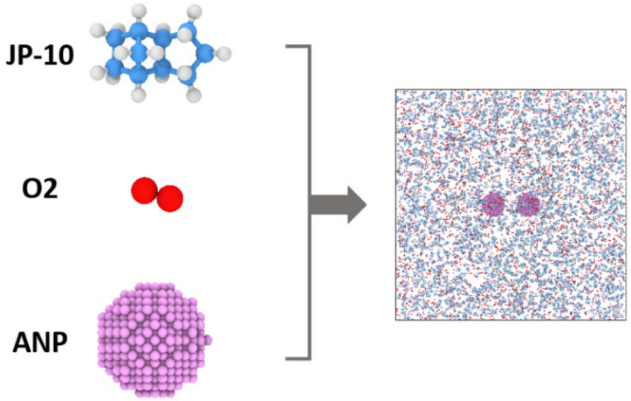

Fig. 3 System configuration of high-energy fuel.

indicating that the melting point of aluminum becomes size-independent above 4 nm, thus mitigating size effects while maintaining computational tractability for ReaxFF-based molecular dynamics simulations.

Oxygen molecules were randomly distributed in the remaining volume of the simulation box not occupied by JP-10 and aluminum particles. To accelerate the reaction process and enhance simulation efficiency, the oxygen density was set significantly higher than under real experimental conditions-a strategy widely adopted in previous combustion simulations.[35,36] To ensure the structural integrity of the aluminum clusters, the number of JP-10 molecules was fixed at a relatively high value; reducing it would require truncating the 4 nm particles to achieve the target aluminum concentration. Meanwhile, to maintain a uniform oxygen environment and ensure sufficient oxidizer for all aluminum loadings, the number of O_2 molecules was set to match that of the highest-concentration system (System 8), providing non-limiting oxygen availability in every case.

System design was tailored to different research objectives. For mechanistic investigations (System 1), a single aluminum particle was placed at the center of the simulation domain. In contrast, concentration-dependent effects were examined using seven additional systems (Systems 2–8) containing increasing numbers of aluminum clusters. All initial configurations were generated using the Packmol package,[37] with a minimum interatomic distance of 2.0 Å enforced to eliminate initial overlap. A detailed summary of the atomic composition and structural parameters of all systems is provided in Table 1. System 1 is used solely for mechanistic illustration and is not included in the concentration-dependent comparisons (Systems 2–8), which share the same O_2 loading. A cubic simulation box was employed, with side lengths of 320 Å for System 1 and 710 Å for Systems 2–8. These volumes were determined based on the prescribed oxygen density.

Table 1 Structural parameters and atomic composition of JP-10/Al/O_2 systems

System	JP-10	Al wt%	Al particle	O_2
1	800	—	1	15 000
2	11 000	10%	2	170 000
3	11 000	15%	3	170 000
4	11 000	20%	4	170 000
5	11 000	25%	6	170 000
6	11 000	30%	7	170 000
7	11 000	35%	9	170 000
8	11 000	40%	11	170 000

3.2 Simulation procedures

As shown in Fig. 4, the entire simulation procedure was divided into four sequential stages: structural relaxation, low-temperature equilibration, heating, and high-temperature combustion. A uniform time step of 0.1 fs was adopted for all stages of the simulation. This multistage design ensures a physically sound and numerically stable transition from the initial configuration to the reactive high-temperature state.

In the first stage, structural relaxation was performed to eliminate local high-energy configurations arising from unreasonable atomic arrangements in the initial structure. Energy minimization was carried out using the conjugate gradient (CG) method under periodic boundary conditions. During energy minimization, the convergence criteria for the total energy and atomic forces were set to 1×10^{-6} kcal mol^{-1} and 1×10^{-6} kcal mol$^{-1}\cdot$Å^{-1}, respectively, consistent with the LAMMPS real unit system. This minimization process does not involve time integration. After optimization, the systems exhibited good energy convergence and physically reasonable configurations, providing a stable foundation for subsequent simulations.

In the second stage, low-temperature equilibration was conducted to establish a thermodynamically consistent initial state while preserving the integrity of the molecular structures. MD was integrated using the velocity-Verlet scheme, with a Berendsen thermostat applied at a constant temperature of 100 K for 50 ps. The primary objective of this stage was to facilitate mechanical and thermal relaxation of the initially constructed system, thereby eliminating artificial high-energy overlaps and local stress concentrations without triggering premature chemical reactions.[38] This procedure ensures that the subsequent high-temperature reactive simulations originate from a physically meaningful and thermodynamically stable state, free from artifacts associated with the initial configuration.

The third stage involved a linear heating process, during which the system temperature was gradually increased from 100 K to the target combustion temperatures (ranging from 2000 K to 4000 K in 500 K increments) at a heating rate of approximately 20 K ps^{-1}. This was achieved by adjusting the heating duration to ensure a continuous and smooth thermal gradient. Specifically, during the initial heating stage from 100 K to 1000 K, the system was evolved under an NVE ensemble combined with the Berendsen thermostat, which was employed as a weak-coupling temperature control method to regulate the heating rate and suppress excessive temperature fluctuations. This strategy helps maintain numerical stability during rapid temperature increase and avoids nonphysical bond breaking

Open Access Article. Published on 20 March 2026. Downloaded on 5/18/2026 10:20:52 PM.
This article is licensed under a Creative Commons Attribution-NonCommercial 3.0 Unported Licence.

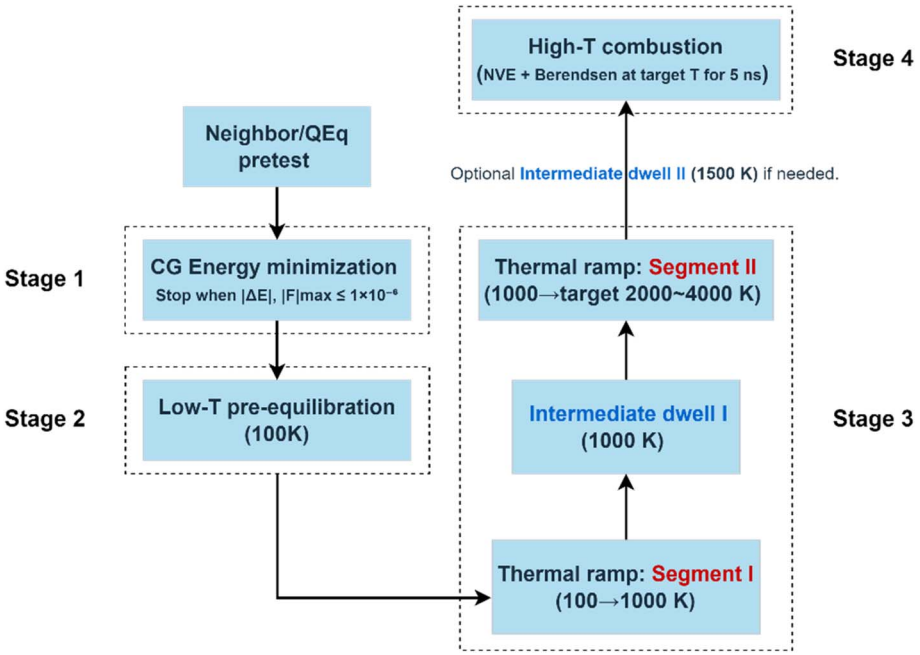

Fig. 4 Flow chart of ReaxFF simulation procedures.

associated with abrupt thermal perturbations.[39,40] Subsequently, the temperature was further increased from 1000 K to the target combustion temperatures under the NVT ensemble, at which point the system had reached sufficient thermal equilibration. All subsequent data collection and statistical analyses were performed exclusively during this NVT-controlled heating stage, ensuring thermodynamic consistency of the reported results. The thermostat parameters were inherited from the previous stage, allowing sufficient thermal diffusion and a uniform temperature distribution throughout the simulation domain. The thermostat settings were inherited from the previous stage, allowing sufficient thermal diffusion and uniform temperature distribution.

The final stage corresponded to the high-temperature combustion process, during which the system was maintained at the combustion temperature for 0.5 ns (5 000 000 steps) to capture the full reaction dynamics, including aluminum oxidation, JP-10 pyrolysis, intermediate species recombination, and final product release. The simulation continued under NVT integration using the Nosé-Hoover thermostat to ensure a rigorous canonical ensemble sampling. Given the highly reactive nature of this stage, bond structures, species compositions, and full atomic trajectories were output every 1000 steps to provide detailed support for kinetic analyses and mechanistic investigations.

4. Results and discussion

4.1 Effect of temperature on the combustion of JP-10/aluminum fuel

4.1.1 Morphological evolution. As shown in Fig. 5, the morphological evolution of aluminum nanoparticles (ANPs) during the combustion process follows a characteristic pathway involving transitions from intact spherical structures to chain-like formations, then to small clusters, and ultimately to large aggregated clusters. At the initial stage, ANPs exhibit dense and well-defined spherical shapes, with only a limited number of oxygen molecules adsorbed on their surfaces, typically captured during the relaxation phase. The structural integrity of the particles remains largely preserved. As the reaction progresses, thermal perturbations and interactions with surrounding reactive species induce surface instabilities, prompting outward migration of aluminum atoms. This leads to the formation of directional chain-like structures, which predominantly extend from the particle edges. In the intermediate stage, these chains undergo fragmentation under elevated temperature and continuous chemical attack, resulting in the generation of numerous small-sized ANP clusters with irregular morphologies. During this period, aluminum atoms no longer exist as intact particles but are instead involved in dynamic processes such as migration, fragmentation, and reaction. As time further evolves, the density of aluminum atoms and small clusters increases, leading to frequent collisions and coalescence events in the system. These interactions promote the formation of large, loosely structured aggregates with blurred boundaries, in which residual chain-like connections are still observed in some regions.

From the perspective of temperature dependence, the morphological evolution of ANPs exhibits clear sensitivity to thermal conditions. At relatively low temperatures (*e.g.*, 2000 K), the initiation of chain formation is delayed, resulting in limited chain elongation and minimal structural disruption. The generation of small clusters is less pronounced, and there is no significant tendency toward aggregation. Under such conditions, most aluminum particles retain their initial compact morphology throughout the simulation. In contrast, at elevated

© 2026 The Author(s). Published by the Royal Society of Chemistry

Open Access Article. Published on 20 March 2026. Downloaded on 5/18/2026 10:20:52 PM.
This article is licensed under a Creative Commons Attribution-NonCommercial 3.0 Unported Licence.

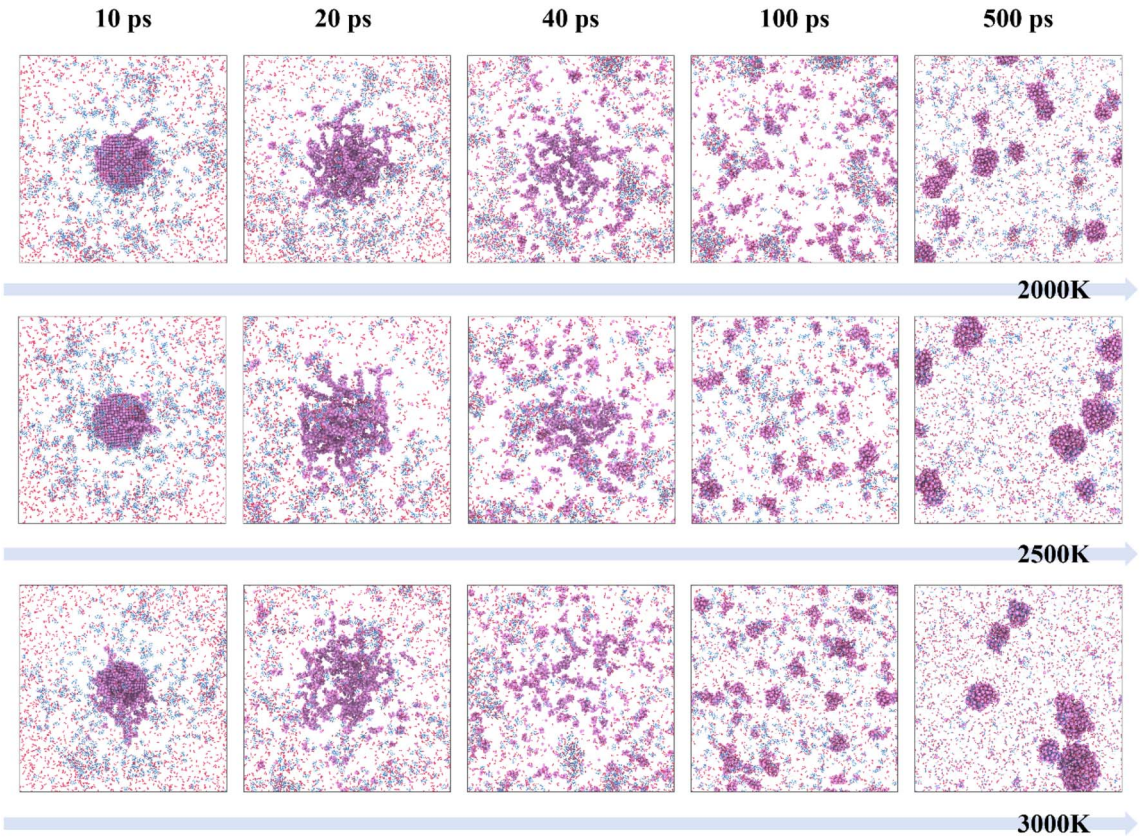

Fig. 5 Morphological evolution of ANPs during the combustion of JP-10/Al fuel at different temperatures.

temperatures, aluminum atoms exhibit markedly enhanced mobility, facilitating earlier nucleation of chain-like structures, which grow longer and become more densely distributed. During the intermediate stage, the number and formation rate of small aluminum clusters increase dramatically. In the late stage, frequent collisions and coalescence events among clusters are observed, ultimately giving rise to large-scale aggregated structures. These high-temperature-induced aggregation processes result in larger and more structurally complex ANP clusters compared to those formed at lower temperatures.

To further quantify these morphological transformations, the temporal variations of cluster number, maximum cluster size, and the radial distribution function (RDF) were analyzed. As shown in Fig. 6(a and b), the maximum size of Al clusters initially decreases due to particle fragmentation, but subsequently increases as aggregation becomes dominant. In contrast, the number of clusters first rises sharply as large particles break into smaller fragments and then declines when these fragments coalesce into larger aggregates. These opposite yet complementary trends provide consistent evidence for the sequential fragmentation-aggregation mechanism governing ANP evolution during combustion.

Meanwhile, the RDF profiles provide atomic-level insight into structural ordering. As illustrated in Fig. 6(c), at the initial stage ($t = 0$ ps), a pronounced sharp peak is observed, indicating strong ordering among aluminum atoms in their crystalline state. In contrast, Fig. 6(d) shows that with the progression of combustion, the peak gradually broadens and lowers in intensity, reflecting the collapse of the initial lattice structure and the transition toward a more disordered, reactive state. These quantitative results corroborate the qualitative observations, highlighting the crucial role of temperature in accelerating cluster restructuring and enhancing atomic-scale disorder.

4.1.2 Ignition delay. To investigate the effect of nano-aluminum particles on the ignition characteristics of JP-10 fuel, Fig. 7 presents the temporal evolution of JP-10 molecular count and its rate of change under different temperature conditions. Specifically, Fig. 7(a) shows the overall trend of JP-10 consumption at 2000 K, 2500 K, and 3000 K for different systems. Under the same temperature, the reactant concentration in the Al-containing system decreases significantly earlier than that in the pure JP-10 system, indicating that the introduction of aluminum particles accelerates the reaction onset. Meanwhile, within the same system, increasing the temperature leads to an earlier consumption of JP-10, reflecting the pronounced promoting effect of high temperature on the pyrolysis rate. To further characterize the ignition behavior more precisely, Fig. 7(b–d) show the first-order derivatives of JP-10 molecular counts with respect to time at 2000 K, 2500 K, and 3000 K, respectively, which represent the consumption rate of the reactant. The negative peak in each plot corresponds to the maximum decomposition rate of JP-10, commonly used to define the ignition delay time. At all temperatures, the Al-

Open Access Article. Published on 20 March 2026. Downloaded on 5/18/2026 10:20:52 PM.
This article is licensed under a Creative Commons Attribution-NonCommercial 3.0 Unported Licence.

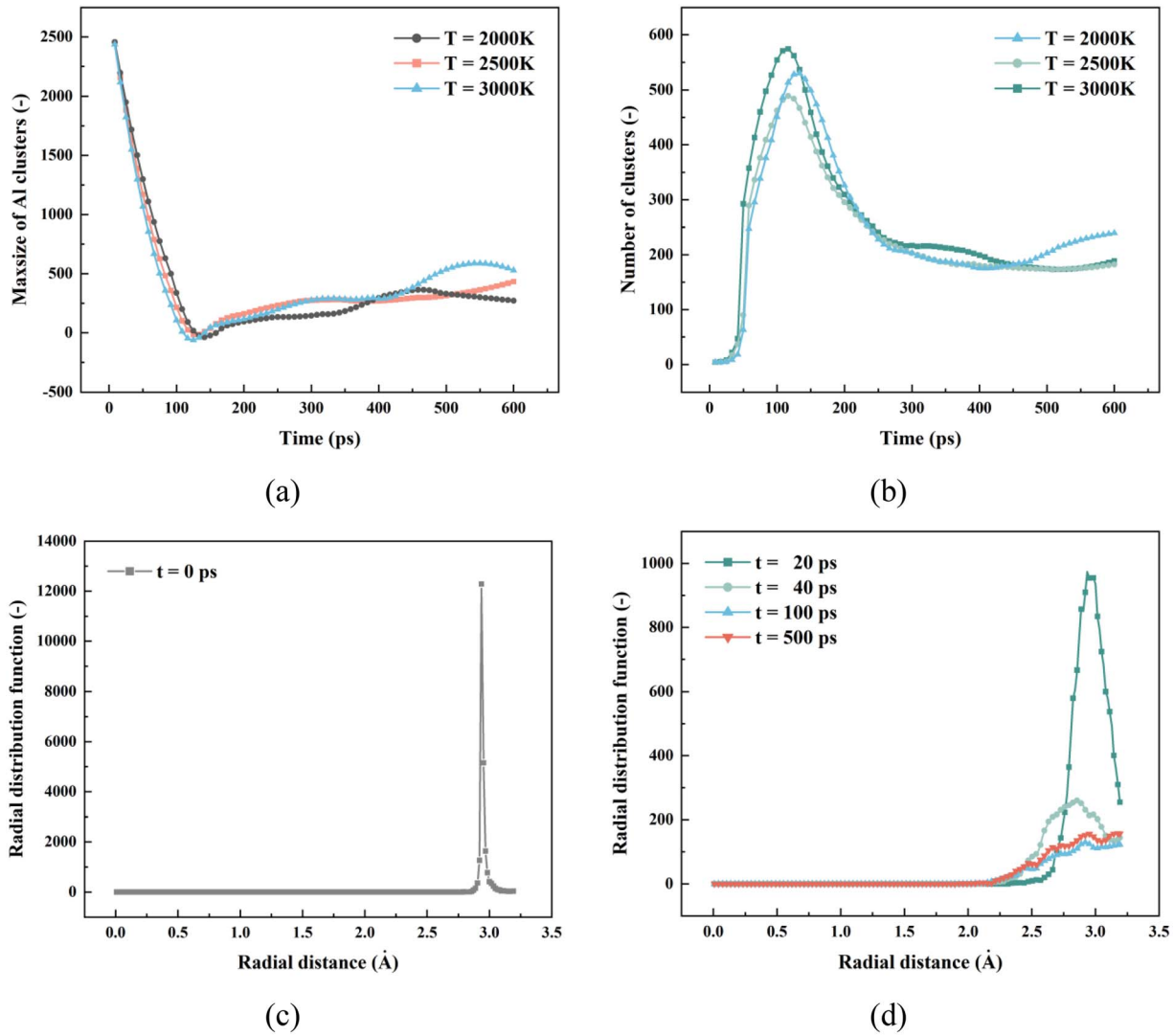

Fig. 6 Quantitative analysis of Al cluster evolution in JP-10/Al systems: (a) temporal variation of maximum cluster size; (b) evolution of cluster number. (c) RDF profile at 0 ps; (d) RDF profiles at later combustion times.

containing systems exhibit earlier negative peaks than the pure JP-10 systems, indicating a significantly accelerated ignition process. Meanwhile, the magnitude of the negative peaks is larger, suggesting that more energy is released during ignition and the reaction is more intense.

At the same time, to further validate the effect of Al particles on ignition delay, the variation in oxygen molecular population was introduced as an additional criterion. As shown in Fig. 8, results display the same tendency as in Fig. 5: at 2000, 2500, and 3000 K, the number of O_2 molecules in the Al-containing systems decreases earlier and at a faster rate than in the pure JP-10 systems. This observation confirms that aluminum particles not only promote the pyrolysis of JP-10 but also accelerate oxidizer consumption, leading to a significantly shortened ignition delay time and a more vigorous combustion onset.

4.1.3 Reaction kinetics analysis. To elucidate the regulatory role of aluminum particles on the reaction pathways and rates of JP-10 combustion, Fig. 9–11 present the evolution of molecular configurations, the cleavage of key chemical bonds, the accumulation of reactive intermediates, and changes in the apparent activation energy. As shown in Fig. 9, the early-stage molecular structure evolution in the JP-10/Al composite system reveals a distinct departure from the initial compact cyclic configuration. In the presence of aluminum, JP-10 molecules exhibit pronounced ring-opening behavior, with many of the originally stable polycyclic structures being dissociated into chain-like or open-ring configurations. This suggests that aluminum significantly promotes main-chain bond cleavage and facilitates structural activation of the fuel precursors.

As shown in Fig. 10(a and b), with the involvement of aluminum particles, the cleavage of primary backbone bonds such as C–C and C–H is significantly accelerated, indicating that JP-10 molecules are rapidly activated into a pyrolysis-ready state at an early stage. Meanwhile, a large number of new O–Al

© 2026 The Author(s). Published by the Royal Society of Chemistry

Open Access Article. Published on 20 March 2026. Downloaded on 5/18/2026 10:20:52 PM.
This article is licensed under a Creative Commons Attribution-NonCommercial 3.0 Unported Licence.

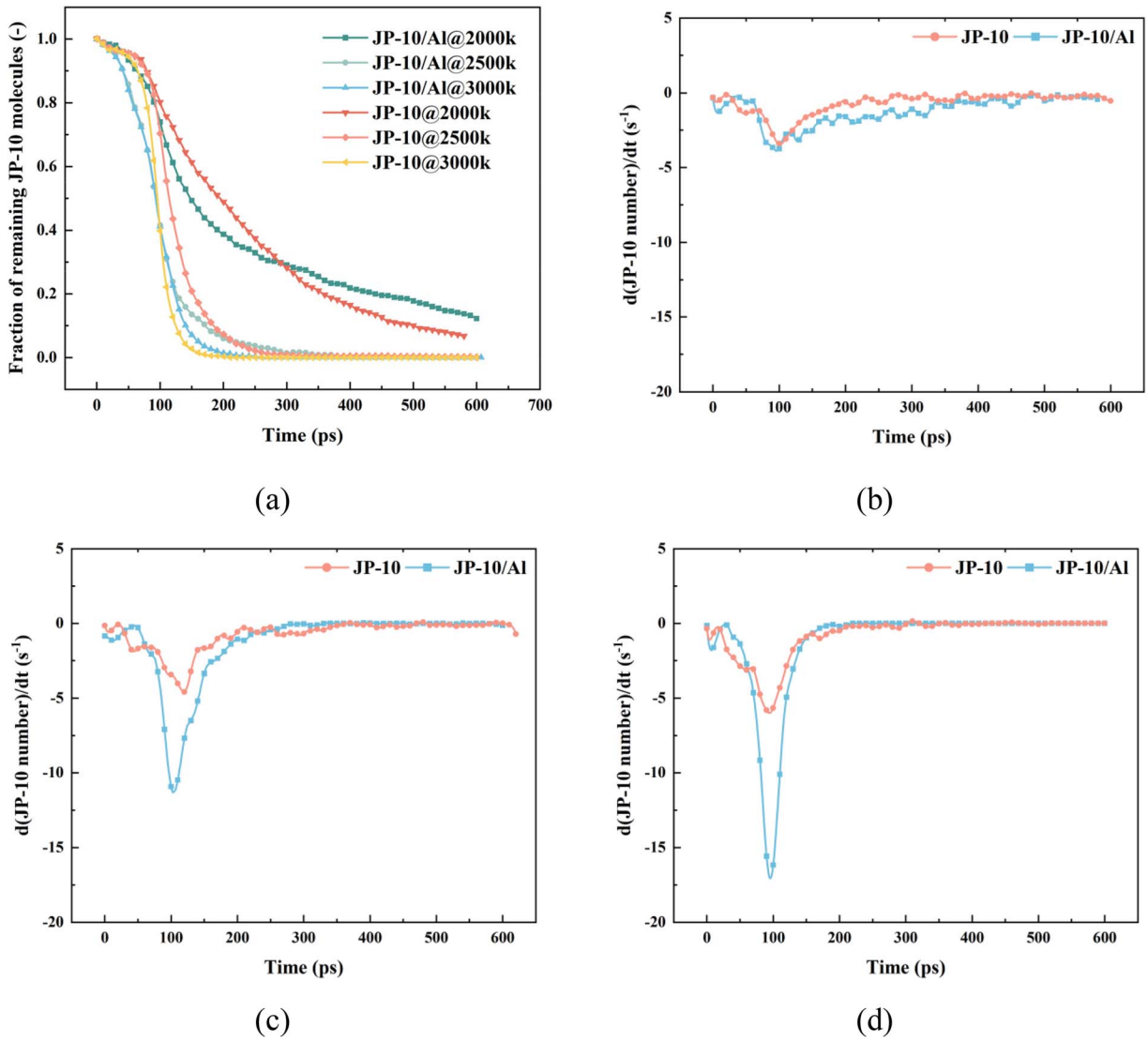

Fig. 7 Analysis of ignition delay in JP-10 and JP-10/Al systems at different temperatures. (a) JP-10 molecular population over time; (b–d) JP-10 consumption rate (d*N*/d*t*) profiles at 2000 K, 2500 K, and 3000 K.

and C–Al bonds are rapidly formed, suggesting that aluminum atoms directly react with surrounding oxygen species and organic fragments. Due to the strong oxygen affinity of aluminum, O_2 is preferentially consumed through rapid Al–O bond formation at the early stage of the reaction. This process significantly reduces the local oxygen availability and weakens the radical-quenching effect of oxygen, thereby shifting the reaction environment toward conditions more favorable for radical accumulation and chain propagation. Under these locally oxygen-lean conditions, dynamically exposed active sites on the aluminum surface remain available to interact directly with JP-10 molecules and reactive intermediates, leading to the formation of transient C–Al interactions. These metal-fuel interactions further weaken the C–C and C–H bonds in JP-10, facilitating molecular cracking and accelerating ring-opening reactions. During this process, reactive aluminum atoms capture oxygen and carbon radicals, thereby promoting the formation of Al–O bonds and releasing localized reaction heat. This enhances the local temperature and reaction-driving force at the molecular level. Regarding the H–Al interactions, although they were observed during the simulations, the statistical analysis shows that they are highly transient. Their frequency and contribution to the overall reaction pathways and energy release are much smaller compared to O–Al and C–Al bonds. Compared to a pure thermal decomposition pathway, this aluminum–mediated bond formation mechanism broadens the available reaction channels and enables oxidation reactions-typically triggered only at higher temperatures-to occur earlier. As a result, the overall reaction pathway is advanced, and coupled reactions are significantly intensified.

This trend is further corroborated by the temporal evolution of intermediate species shown in Fig. 10(c and d). In the JP-10/Al system, reactive fragments such as OH, O, CO_2, and H_2O are generated in large quantities at an early stage, indicating that

Open Access Article. Published on 20 March 2026. Downloaded on 5/18/2026 10:20:52 PM.
This article is licensed under a Creative Commons Attribution-NonCommercial 3.0 Unported Licence.

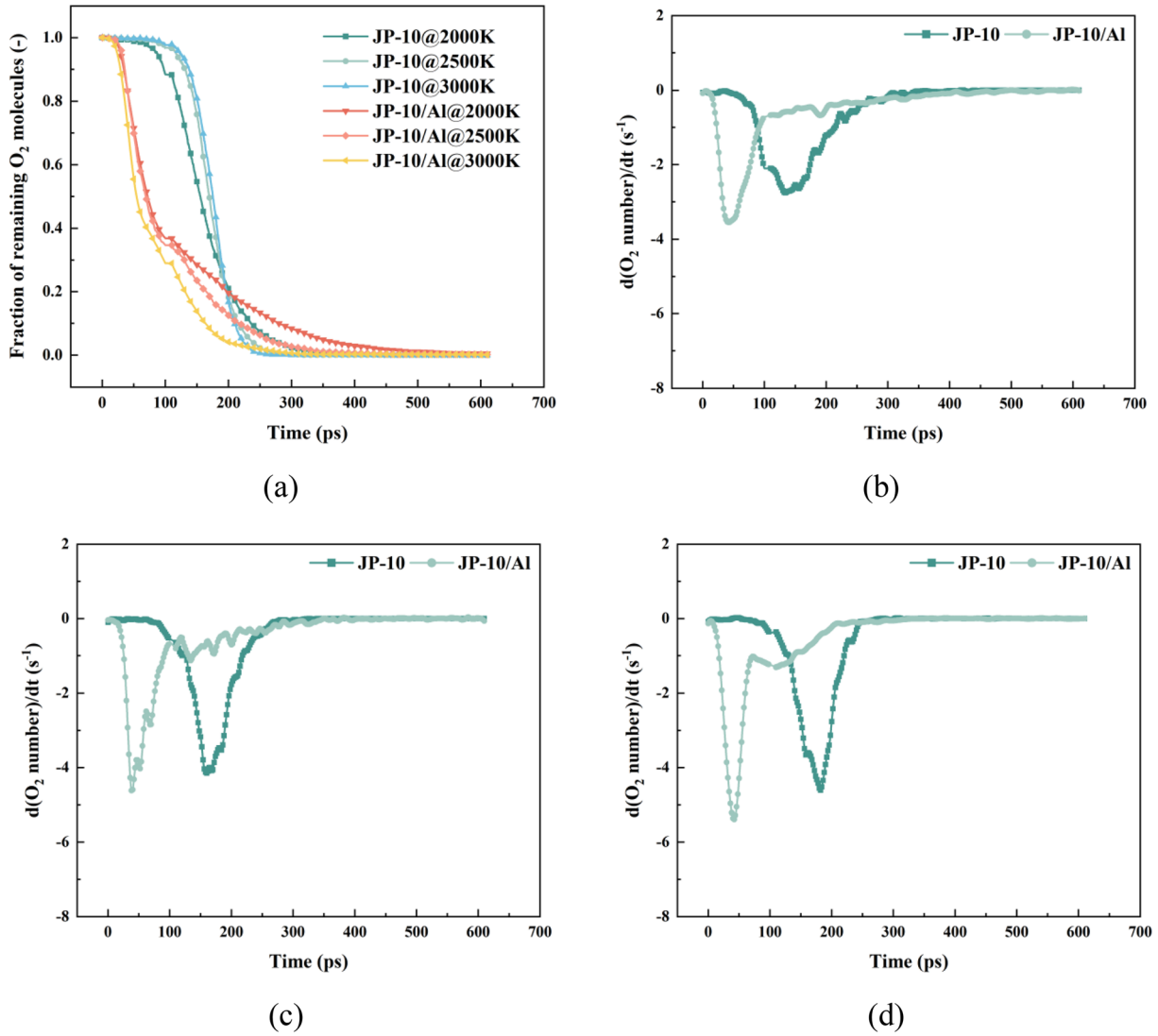

Fig. 8 Analysis of ignition delay in JP-10 and JP-10/Al systems at different temperatures. (a) O_2 molecular population over time; (b–d) O_2 consumption rate (d*N*/d*t*) profiles at 2000 K, 2500 K, and 3000 K.

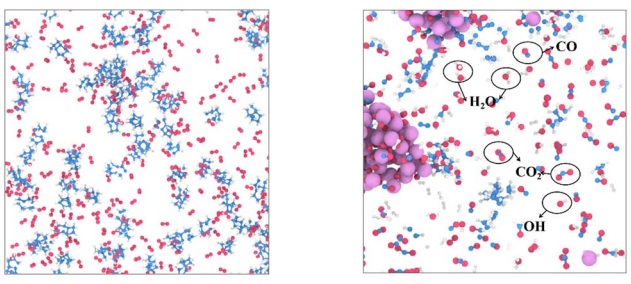

Fig. 9 Molecular structure evolution of JP-10: (a) JP-10 system; (b) JP-10/Al system.

oxidation reaction chains are rapidly initiated. Among them, OH and O are typical radical-chain participants; their early accumulation may significantly enhance chain propagation efficiency, promoting the transition of JP-10 into the decomposition–oxidation stage. Additionally, the earlier appearance of larger carbon-containing fragments such as CO and CHO suggests that intermediate steps following C–C bond cleavage are accelerated, effectively shortening the time window between thermal decomposition and final oxidation.

To quantify the regulatory effect of aluminum particles on the combustion reaction barrier, the rate constants of both systems at different temperatures were fitted, and the corresponding apparent activation energies were extracted, as shown in Fig. 11. The activation energy for the JP-10/Al system is 14.03 kJ mol^{-1}, representing a reduction of approximately 49.8% compared to the pure JP-10 system (27.96 kJ mol^{-1}). This result is consistent with the aforementioned microscopic reaction behaviors, indicating that the addition of aluminum reduces the reaction energy barrier through multiple mechanisms. Specifically, the presence of aluminum promotes the ring-opening of JP-10 molecules, enhancing the efficiency of initial bond dissociation; the increased cleavage rates of C–C

© 2026 The Author(s). Published by the Royal Society of Chemistry

Open Access Article. Published on 20 March 2026. Downloaded on 5/18/2026 10:20:52 PM.
This article is licensed under a Creative Commons Attribution-NonCommercial 3.0 Unported Licence.

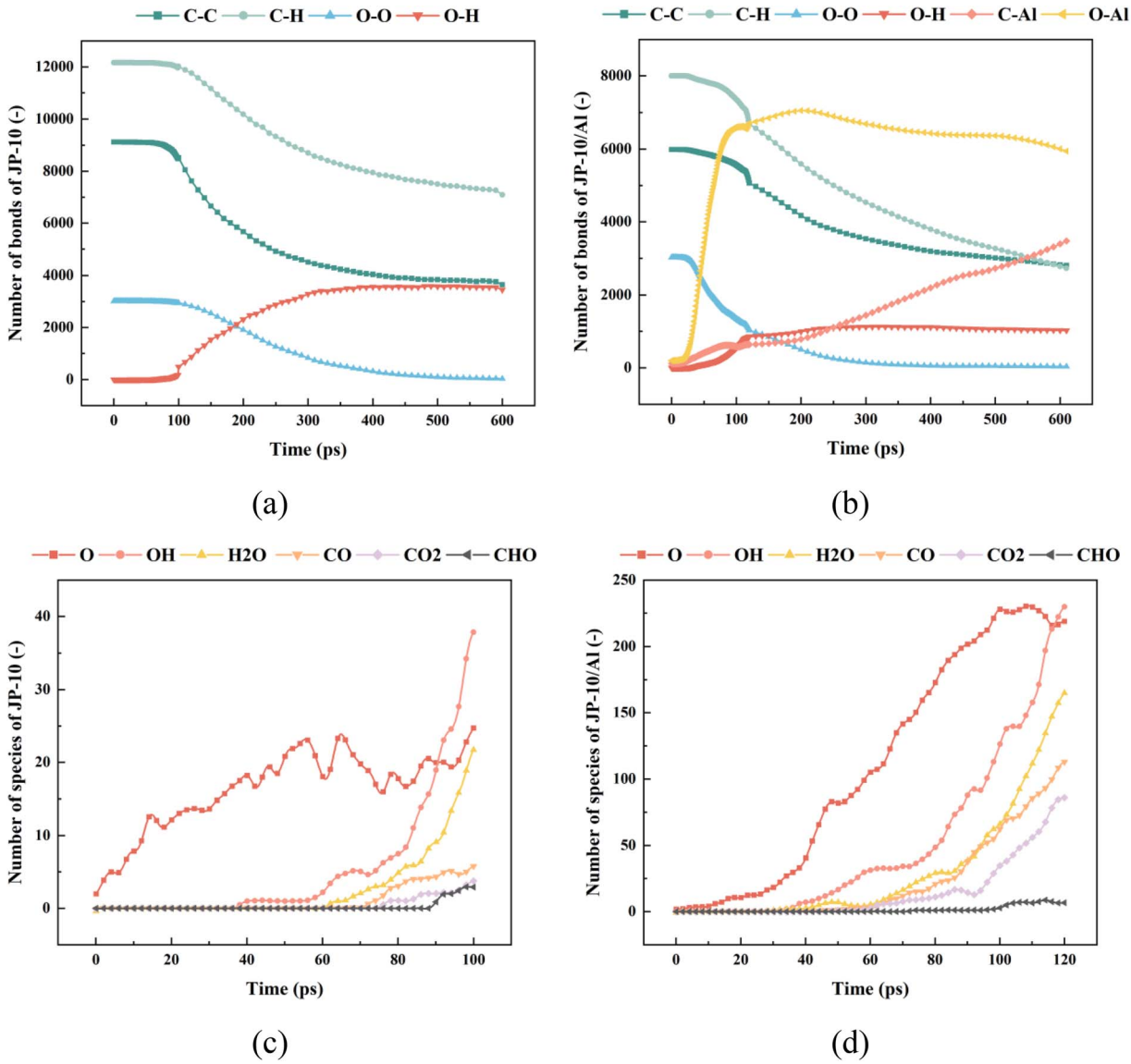

Fig. 10 Temporal evolution of chemical bond types and major reaction intermediates: (a) time-dependent changes in bond populations of JP-10 system; (b) time-dependent changes in bond populations of JP-10/Al system; (c) generation of key reactive species of JP-10 system; (d) generation of key reactive species of JP-10/Al system.

and C–H bonds, along with the rapid formation of O–Al and C–Al bonds, mark the early onset of oxidation pathways. Additionally, the rapid accumulation of key radicals and products such as OH, O, and CO_2 further accelerates the propagation of chain reactions. These synergistic changes at the molecular structure, bond, and species levels collectively contribute to the reduction in activation energy by affecting the rate-limiting steps.

4.2 Effect of ANP concentration on the combustion of JP-10/Al fuel

To evaluate the regulatory effect of aluminum nanoparticle (ANP) concentration on the combustion reaction of JP-10, this section presents comparative simulations of JP-10/Al composite systems with mass fractions ranging from 10% to 40%, focusing on the formation behavior of O–Al bonds and the variation in JP-10 molecular consumption.

As depicted in Fig. 12, increasing the aluminum concentration significantly alters the initial spatial distribution of particles. In high-concentration systems, the average interparticle distance is substantially reduced, promoting frequent contact and adsorption under thermal excitation. This leads to pronounced aggregation behavior at the early stage of the reaction. The aggregation process initially manifests as local bridging between adjacent particles, followed by continuous expansion of the interface, evolving into elongated, non-spherical transitional structures. Eventually, these structures transform into large, spherical clusters with compact surfaces and regular contours. From a morphological evolution perspective, the aggregation behavior observed here exhibits

Open Access Article. Published on 20 March 2026. Downloaded on 5/18/2026 10:20:52 PM. This article is licensed under a Creative Commons Attribution-NonCommercial 3.0 Unported Licence.

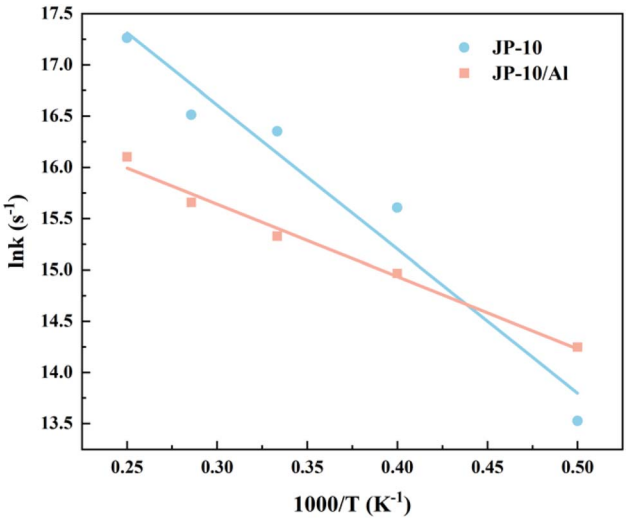

Fig. 11 Arrhenius plots of reaction rate constants for JP-10 and JP-10/Al systems.

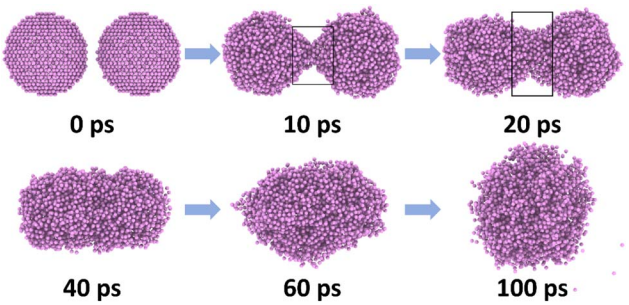

Fig. 12 Aggregation behavior of aluminum nanoparticles at high concentration.

features analogous to a sintering-like aggregation mechanism. Previous study[24] on aluminum nanoparticle combustion have reported that, under high-temperature reactive environments, nanoparticle aggregation often proceeds through contact-induced bridging and subsequent interface growth, resembling sintering-driven particle coalescence. In the present simulations, although bare aluminum nanoparticles are initially employed, partial local oxidation structures may form on particle surfaces during the relaxation stage. Upon heating and combustion, neighboring particles first establish bridge-like contacts, followed by rapid interface expansion driven by localized exothermic reactions at the contact regions. This reaction-induced growth process results in elongated transitional structures that subsequently evolve into larger, compact, and approximately spherical clusters. It is important to note that this aggregation behavior differs fundamentally from classical thermal sintering controlled by bulk diffusion or melting. Instead, the aggregation is dominated by chemical reactions, surface evolution, and interfacial heat release during combustion. Therefore, the observed process is more appropriately characterized as a reaction-induced, sintering-like aggregation mechanism under combustion conditions. Throughout the thermal reaction stage, these clusters remain stable without significant fragmentation or dispersion. From the perspective of reaction kinetics, the formation of large clusters suppresses oxidation efficiency. On one hand, aggregation dramatically reduces the specific surface area of the aluminum particles, decreasing the number of active sites available for oxygen adsorption and reaction per unit volume. On the other hand, the compact structure of the spherical clusters shields the internal aluminum atoms, hindering oxygen diffusion into the core region-exhibiting a typical "diffusion-limited" characteristic.

The quantitative results in Fig. 13(a) and (b) further support this inference. In Fig. 13(a), the vertical axis represents the

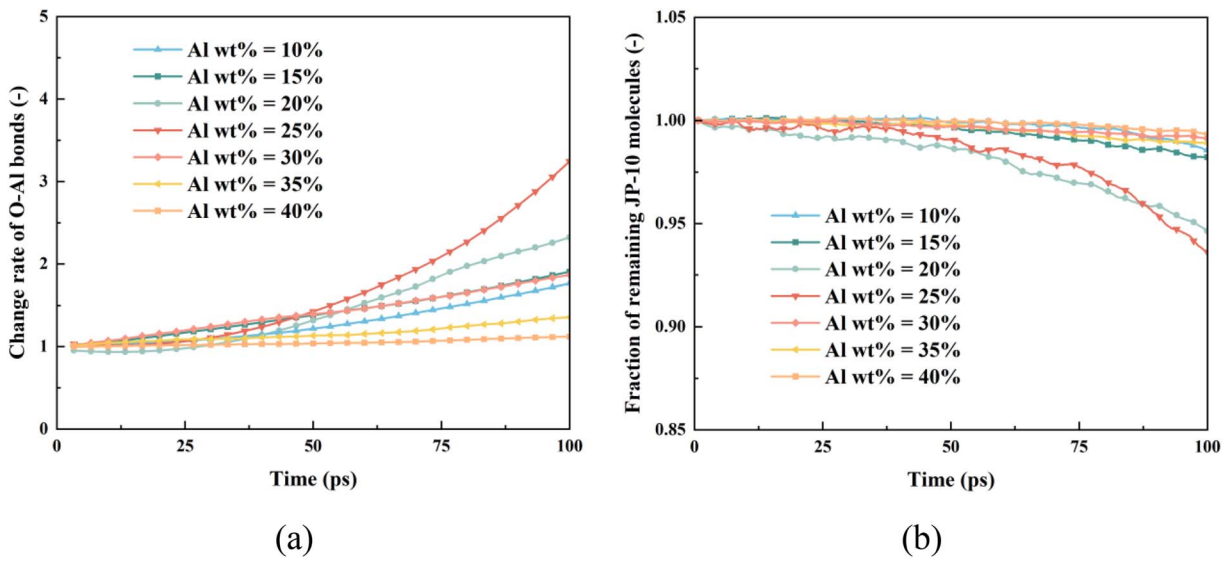

Fig. 13 Effect of ANP concentration on the combustion of JP-10/Al fuel: (a) temporal evolution of O–Al bond populations at different aluminum concentrations; (b) decomposition profiles of JP-10 molecules at different aluminum concentrations.

© 2026 The Author(s). Published by the Royal Society of Chemistry

Open Access Article. Published on 20 March 2026. Downloaded on 5/18/2026 10:20:52 PM. This article is licensed under a Creative Commons Attribution-NonCommercial 3.0 Unported Licence.

normalized change rate of O–Al bond counts, which is a dimensionless quantity. Specifically, the O–Al bond number is normalized with respect to its value at the end of the initial equilibration stage. As discussed previously, a small number of O–Al bonds inevitably form during the initial thermal relaxation process. To eliminate the influence of this non-zero initial value and to enable a more direct comparison of the incremental oxidation behavior under different aluminum concentrations, the bond evolution data were normalized accordingly. The formation rate of O–Al bonds reaches a maximum at 20–25 wt% Al concentration, indicating that oxidation is most active in this range. In contrast, for systems with 35–40 wt% Al, the growth of O–Al bonds slows down considerably, despite the higher aluminum content, suggesting that cluster formation limits effective oxygen utilization. Simultaneously, JP-10 degradation also proceeds faster at moderate Al concentrations, which may be attributed to the enhanced thermal feedback from the exothermic oxidation reactions. In higher-concentration systems, this synergistic effect is diminished due to the suppressed reactivity of aggregated aluminum.

Therefore, although increasing aluminum content raises the reductant level in the system, exceeding a certain threshold leads to reduced combustion efficiency due to interfacial loss, reactivity constraints, and mass transport limitations caused by aggregation. Considering both reaction rate and structural evolution, 20–25 wt% is identified as the optimal aluminum concentration window for the present system.

5. Conclusion

This study employed reactive molecular dynamics (ReaxFF MD) simulations to investigate the ignition and combustion characteristics of JP-10/Al composite fuels under different thermal and compositional conditions. The major findings can be summarized as follows:

(1) The morphological evolution of Al nanoparticles exhibits a characteristic pathway of chain-like extension, fragmentation, and secondary aggregation, with transition rates strongly dependent on temperature. These structural transformations directly affect surface reactivity and the accessibility of oxygen.

(2) At the macroscopic scale, the addition of Al nanoparticles accelerates JP-10 consumption and markedly shortens ignition delay. At the microscopic level, the promotional effect originates from coupled processes: the rapid formation of Al–O and Al–C bonds destabilizes JP-10 and facilitates cage ring-opening, while the accelerated generation of reactive fragments reduces the apparent activation energy by 49.8%.

(3) Concentration dependence reveals a trade-off between ignition promotion and aggregation. Low-to-moderate Al loadings enhance combustion by increasing reactive surface area and fragment production, whereas excessive additions lead to severe aggregation and diminished efficiency. An optimal concentration window of 20–25 wt% was identified as balancing ignition promotion with minimized aggregation losses.

The present work clarifies the molecular mechanisms by which Al regulates the ignition behavior of JP-10, quantitatively establishes its effects on ignition delay and activation energy, and identifies a rational loading window for improved combustion efficiency. Future efforts will extend this framework to multi-component gel fuel systems and combustion-relevant environments, enabling predictive design of advanced composite fuels for aerospace propulsion.

Author contributions

Mengfan Si: methodology, investigation, formal analysis, data curation, visualization, writing – original draft. Shuai Wang: writing – review & editing, supervision, resources. Haiou Wang: writing review & editing. Hanhui Jin: writing – review & editing. Kun Luo: resources. Jianren Fan: conceptualization, funding acquisition, project administration, supervision, resources.

Conflicts of interest

There are no conflicts of interest to declare.

Data availability

The data supporting this article have been included in the article and as part of the supplementary information (SI). Supplementary information is available. See DOI: https://doi.org/10.1039/d6ra00051g.

Acknowledgements

We are grateful for the support from the National Natural Science Foundation of China (grant no. U2341283).

References

1 X. Wang, J. Zhang, Y. MA, G. Wang, J. Han, M. Dai and Z. Y. Sun, *Appl. Surf. Sci.*, 2020, **504**, 144581.
2 D. Liang, Z. Wu, Y. Jiang, K. Ren, M. Zhou, S. Chu and D. Shen, *SSRN Electron. J.*, 2022, **398**, 117108.
3 Y. Luo, X. Xu, J. Zou and X. Zhang, *J. Propul. Power*, 2016, **32**, 1167–1177.
4 Y. Jin, S. Dou, Q. Yang, X. Xu, Q. Fu and L. Pan, *Acta Astronaut.*, 2021, **185**, 70–77.
5 M. S. Gad, S. M. Abdel Razek, P. V. Manu and S. Jayaraj, *Adv. Mech. Eng.*, 2021, **13**, 752157198.
6 A. Mostafa, M. Mourad, A. Mustafa and I. Youssef, *Energy Conv. Manag. X*, 2023, **19**, 100389.
7 Y. Chen, K. Xue, Y. Liu, L. Pan, X. Zhang and J. Zou, *Chin. J. Chem. Eng.*, 2024, **65**, 230–242.
8 W. Yang, J. Wang, B. Zhu and Y. Sun, *J. Therm. Anal. Calorim.*, 2025, **150**, 13169–13180.
9 M. Zhang, H. Li, R. Li, B. Ni, J. Chen, B. Zhu and Y. Sun, *Combust. Flame*, 2026, **284**, 114700.
10 T. Yang, X. Qian, J. Dai, J. Liu, J. Chen, J. Wang, M. Xu, Y. Sun and B. Zhu, *Combust. Flame*, 2024, **264**, 113442.
11 H. S. Sim, S. Jekal, C. Yoon and S. L. Hong, *Prog. Org. Coat.*, 2025, **205**, 109289.
12 M. Chen, W. Li, H. Zhang, M. Liu, J. Zhang, X. Li and Y. Han, *Energy Adv.*, 2023, **2**, 54–72.

© 2026 The Author(s). Published by the Royal Society of Chemistry

Open Access Article. Published on 20 March 2026. Downloaded on 5/18/2026 10:20:52 PM. This article is licensed under a Creative Commons Attribution-NonCommercial 3.0 Unported Licence.

13 M. Feng, H. Li, Q. Mao, K. H. Luo and P. Hellier, *J. Phys. Chem. C*, 2019, **123**, 24436–24445.
14 Z. Wang, Y. Ma, P. Zheng, J. Qian, M. Fu, Y. Jiang, W. Wu and H. Li, *J. Mater. Sci.*, 2024, **59**, 5414–5425.
15 L. Song, T. Zhang, Y. Zhang, B. Chen, M. Wu, S. Zhou and Z. Mei, *Mater. Today Commun.*, 2023, **35**, 106180.
16 X. Jiang, Y. Hu, L. Ling and X. Wang, *Appl. Surf. Sci.*, 2021, **548**, 149159.
17 F. Xiong, B. Zhu, C. Jiang, C. Su, J. Liu, J. Chen, M. Xu and Y. Sun, *Thermochim. Acta*, 2025, **749**, 180002.
18 Y. R. Zhang, A. C. T. van Duin and K. H. Luo, *Fuel*, 2018, **234**, 94–100.
19 Y. Cheng, Y. Zhao, F. Zhao, S. Xu, X. Ju and C. Ye, *Fuel*, 2022, **330**, 125465.
20 Y. Cheng, F. Zhao, S. Xu, X. Ju and Y. Zhao, *Fuel*, 2023, **339**, 127438.
21 Y. Zhao, X. Wang, Y. Cheng, Z. Mei, X. Chen and S. Tang, *Fuel*, 2024, **358**, 130047.
22 Y. Lu, J. Chen, B. Zhu, J. Wang, C. Jiang, M. Xu and Y. Sun, *Colloids Surf., A*, 2023, **678**, 132459.
23 Z. Kong, Y. Lu, J. Dai, Y. Sun, J. Chen and B. Zhu, *Mater. Today Chem.*, 2025, **50**, 103150.
24 X. Zhao, Z. Wang, Y. Sun, Y. Zhang, Z. Zhang and J. Xiao, *Colloids Surf., A*, 2024, **701**, 134918.
25 B. Chen, S. Shan, H. Liu, J. Liu and Q. Yang, *Acta Astronaut.*, 2023, **208**, 256–269.
26 A. C. T. van Duin, S. Dasgupta, F. Lorant and W. A. Goddard, *J. Phys. Chem. A*, 2001, **105**, 9396–9409.
27 K. Chenoweth, A. C. T. van Duin and W. A. Goddard, *J. Phys. Chem. A*, 2008, **112**, 1040–1053.
28 E. C. Neyts, K. Ostrikov, Z. J. Han, S. Kumar, A. C. T. van Duin and A. Bogaerts, *Phys. Rev. Lett.*, 2013, **110**, 65501.
29 M. Raju, A. C. T. van Duin and K. A. Fichthorn, *Nano Lett.*, 2014, **14**, 1836–1842.
30 M. C. Hatzell, M. Raju, V. J. Watson, A. G. Stack, A. C. T. van Duin and B. E. Logan, *Environ. Sci. Technol.*, 2014, **48**, 14041–14048.
31 N. Onofrio, D. Guzman and A. Strachan, *Nat. Mater.*, 2015, **14**, 440–446.
32 S. G. Srinivasan, A. C. T. van Duin and P. Ganesh, *J. Phys. Chem. A*, 2015, **119**, 571–580.
33 S. Hong and A. C. T. van Duin, *J. Phys. Chem. C*, 2016, **120**, 9464–9474.
34 J. Liu, M. Wang and P. Liu, *Mater. Res. Express*, 2018, **5**, 65011.
35 P. Liu, J. Liu and M. Wang, *Combust. Flame*, 2019, **201**, 276–289.
36 B. Wu, F. Wu, P. Wang, A. He and H. Wu, *J. Phys. Chem. C*, 2021, **125**, 11359–11368.
37 L. Martinez, R. Andrade, E. G. Birgin and J. M. Martinez, *J. Comput. Chem.*, 2009, **30**, 2157–2164.
38 B. D. Jensen, A. Bandyopadhyay, K. E. Wise and G. M. Odegard, *J. Chem. Theory Comput.*, 2012, **8**, 3003–3008.
39 H. J. C. Berendsen, J. P. M. Postma, W. F. van Gunsteren, A. DiNola and J. R. Haak, *J. Chem. Phys.*, 1984, **81**, 3684–3690.
40 D. Wu, H. Dong, J. Luan, Q. Du, J. Gao, D. Feng, Y. Zhang, Z. Zhao and D. Li, *Energies*, 2023, **16**, 6186.

© 2026 The Author(s). Published by the Royal Society of Chemistry